Pergamon

Solid State Communications, Vol. 107, No. 10, pp. 547–551, 1998
© 1998 Elsevier Science Ltd
Printed in Great Britain. All rights reserved
0038–1098/98 $19.00+.00

PII: S0038–1098(98)00281-6

RAMAN SCATTERING IN TERNARY $AlAs_xSb_{1-x}$ FILMS

H.C. Lin,* J. Ou, C.H. Hsu, W.K. Chen and M.C. Lee

Department of Electrophysics, National Chiao Tung University, Hsinchu, Taiwan 300, People's Republic of China

(*Received* 22 *April* 1998; *accepted* 26 *May* 1998 *by Z.Z. Gan*)

Thin films of the ternary $AlAs_xSb_{1-x}$ alloys, prepared by metalorganic chemical vapor deposition, were studied by Raman scattering. The Raman shifts show one-mode behavior and the forbidden TO phonon scattering is observable due to the relaxed selection rule. Our results of the mixed compounds can be interpreted using the spatial correlation model. Moreover, the enhanced scattering was observed at 2.15 and 2.8 eV which are attributable to the E_0 and E_1 transitions of AlAs and AlSb. © 1998 Elsevier Science Ltd. All rights reserved

Keywords: A. semiconductors, A. thin films, D. optical properties, D. phonons.

Tunability of the semiconductor bandgap energy has long been pursued for optoelectronic uses [1, 2]. The ternary $AlAs_xSb_{1-x}$ alloy is such material that shows promising applications in near infrared detection, laser diodes and resonant tunneling diodes, because of its large heterojunction conduction-band offset, low refractive index (3.0) and high Γ-band gap (2.6 eV @$x = 0.45$) [3, 4]. However, it is difficult to grow AlAsSb ternary compounds over an entire composition range, since they are thermodynamically immiscible, hygroscopic and reactive with oxygen. So far there appear a few reports by employing the metalorganic chemical vapor deposition (MOCVD) method, yet with limited composition range [5, 6]. To our best knowledge, the Raman study of such alloy is still rare that its characterization is necessary [7]. In this study, we carried out the Raman measurements of the MOCVD grown $AlAs_xSb_{1-x}$ films. In contrast to the "one + two" mode behavior of InAsSb and two-mode behavior of AlGaSb and InPSb [8–10], our results show just "one mode" behavior over the whole composition range. The phonon spectra exhibit linear change with the solid composition that is different from the nonlinear variation reported by Sela *et al.* [7]. By applying the spatial correlation model [11, 12], the simulated Raman line shapes for different compositions show good fit to the measured spectra. Besides, we observed resonant scattering that is believed to be associated with interband transitions across the Γ and X critical points.

The AlAsSb samples were grown by the MOCVD method using trimethylaluminum (TMAl), tertiarybutylarsine (TBAs) and trimethylantimony (TMSb) sources. We succeeded in depositing an entire composition range of $AlAs_xSb_{1-x}$ films on (1 0 0) GaAs substrate with different input As/Sb gas mixtures at 600–625°C [13]. The composition x is determined with an uncertainty less than ± 0.07 by double crystal X-ray measurements. The linewidth is typically 500–1000 arc sec. Lattice mismatch on the interface is estimated to be ~0 and 8.6% for pure AlAs and AlSb, respectively. The as-grown film has a typical thickness of 2 to 4 μm and a cap layer of ~150 nm to prevent hygroscopic effect and fast Al oxidation. We used GaP cap for $x < 0.8$, because it is more transparent to the probe wavelength than GaAs cap which was used for $x > 0.8$ to avoid confusion between AlAsSb modes (340–402 cm^{-1}) and the GaP phonon modes (367/403 cm^{-1}). Raman system consists of a double monochromator (Jobin Yvon U1000) and a multichannel diode array detector (Princeton Instruments IRY1024). The spectral resolution was about 2–4 cm^{-1}. The laser power was about 25 mW on the samples and the Raman signals were collected in the backscattering geometry. For resonance study, a He–Cd laser, a mixed Ar^+/Kr^+ ion laser and a ring dye laser tuning in the R6G range were used to cover from 441.6 to 647.1 nm.

As formed by binary systems of AlAs and AlSb, the ternary $AlAs_xSb_{1-x}$ alloy also has the zincblende structure

* Corresponding author. E-mail: u832/802@cc.nctu.edu.tw

with some internal strain. Its symmetry is characterized by the T_d point group. Using the backscattering geometry with both incident and scattered beams polarized along (0 1 1) direction, the LO mode belonging to Γ_{15} representation is the only allowed transition in the first-order Raman process [14]. Our Raman spectra for different compositions of $AlAs_xSb_{1-x}$ epilayers are shown in Fig. 1 by using the 514.5 nm probe wavelength. The S/N ratio of pure AlAs ($x = 1$) spectrum is good and the LO intensity is much larger than the TO's as normally seen in the bulk material. However, for pure AlSb ($x = 0$), both the LO and TO modes appear but show weaker intensity and broader width than AlAs. The presence of TO mode could be attributed to the disorder-activated scattering from imperfections formed during the deposition process due to lattice-mismatch [15]. Besides, we found that the deficiency of TMAl supply during the growth can cause a similar effect. It is verified that the normal situation ($I_{TO} \ll I_{LO}$) reappears by increasing the TMAl final rate by ~55%. For the mixed $AlAs_xSb_{1-x}$ alloys ($1 > x > 0$), the selected rule no longer holds that renders even larger TO scattering. Especially for x between 0.4 and 0.7, the TO's intensity becomes comparable to the LO's due to the severely reduced symmetry. Not only so, the enhanced LO and TO scattering can also take place when the excitation wavelength approaches the resonance conditions of the mixed ternary alloys. We will discuss the resonance effect later.

Concerning the Raman shift and its full width at half maximum (FWHM) of $AlAs_xSb_{1-x}$, we obtained the information from two Lorentzian functions that depict

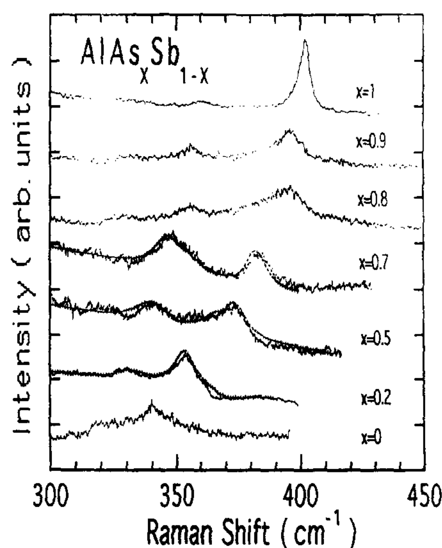

Fig. 1. Raman spectra of $AlAs_xSb_{1-x}$ obtained by 514.5 nm laser wavelength. Cross hatched curves are simulated by the spatial correlation model (see text).

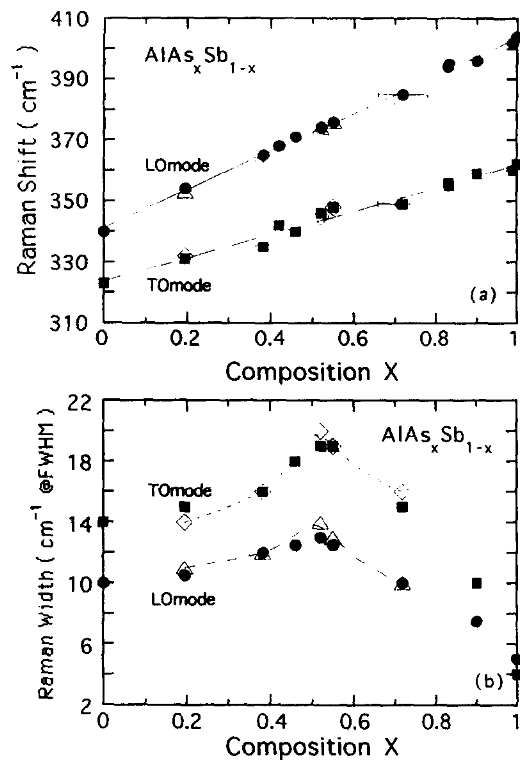

Fig. 2. (a) LO and TO Raman shifts (filled symbols) of $AlAs_xSb_{1-x}$ vary linearly with the solid composition x and the so-called "one mode" behavior. (b) Line widths (filled symbols) show large broadening due to alloying disorder. The spatial correlation accounts well for shifts and broadenings of $0.7 > x > 0.2$ (open symbols).

both TO and LO phonons. Their dependence on the solid composition x are drawn in Figs 2(a) and 2(b) by the filled symbols. One can see almost straight lines for both TO and LO modes, with respective slopes of 4 and 6.5 cm^{-1} per 10% increment in As composition. They appear to be different from the nonlinear shift variation of AlAsSb reported by Sela *et al.* [7] and suggest linear changes in the lattice spacing by randomly mixing As and Sb in the alloy. Between pure AlSb and AlAs, the Raman shift is from 322 to 361 cm^{-1} for the TO mode and 340 to 402 cm^{-1} for the LO mode. Such differences (39 to 62 cm^{-1}) are not too large that is the necessary condition for the "one mode" behavior, since As and Sb masses are much heavier than Al mass [16]. We belive that the chemical environment (due to molar content variations) is critical for determining the phonon frequency.

The FWHMs of Raman lines are analyzed and denoted by the filled symbols in Fig. 2(b). For nearly pure AlAs ($x \sim 1$), both LO and TO modes are about 4 cm^{-1} wide which is close to the intrinsic value, because of nearly perfect lattice matching. However, for pure AlSb ($x = 0$), they become as large as 10–14 cm^{-1}. It is also attributable to the structural disorder (lattice

relaxation) caused by large lattice mismatch (~8.6%) between the AlSb epilayer and GaAs substrate. For the alloy compositions x between 0.2 and 0.8, the linewidth broadens monotonously towards $x \sim 0.5$ with a peak value of 20 and 13 cm^{-1} for the TO and LO modes, respectively. Such behavior is commonly seen in many kinds of mixed compounds because of alloy disorder. The long-range translational invariance is destroyed by both group-V elements alloying and the increasing lattice mismatch from introduction of Sb atom into AlAs structure. The momentum conservation no longer holds strictly but relaxes significantly that makes various excitation routes possible.

We also applied the spatial correlation model to fit the Raman lineshapes with the following Voigt formula integrated over reciprocal lattice (q) in the Brillouin zone, [11, 12]

$$I(\omega) \propto \int \left(\frac{e^{-(qL/4)^2 4\pi q^2}}{(\omega - \omega_{LO}(q))^2 + \left(\frac{\Gamma_{LO}}{2}\right)^2} + \frac{e^{-(qL/4)^2 4\pi q^2}}{(\omega - \omega_{TO}(q))^2 + \left(\frac{\Gamma_{TO}}{2}\right)^2} \right) dq \quad (1)$$

Here Γ_{LO} and Γ_{TO} are intrinsic widths of the LO and TO modes, respectively. $\omega_{LO}(q)$, $\omega_{TO}(q)$ are the dispersion relations of the mixed phonon modes which assume the cosine form. For simplicity, we also assume a spherical symmetry for integration over q variable. The Gaussian distribution expresses the contribution from different-sized clusters in which the correlation length (L) is an adjustable parameter that accounts for the variation in solid composition x. The correlation length is found to play more important role than the dispersion relations since they are smooth curves. The calculated results, shown by the cross-hatched curves in Fig. 1 and the open symbols in Figs 2(a) and 2(b) for different compositions, show good fits to the measurements. For the intermediate compositions, we obtained correlation lengths ranging from 7 to 15 lattice constants. That indicate worse crystallinity as compared to the long range order of AlAs binary compounds whose correlation length is about 80 lattice constants. Thus, wide Raman widths are mainly resulted from imperfect translational symmetry.

As for the resonant Raman results of AlAsSb, most excitation wavelengths used in our experiments (647 to 442 nm) involve band to band transitions, since the fundamental band gap energies of AlAsSb alloys range from 1.61 to 2.15 eV (or 770 to 577 nm). In general, the scattered intensity from the shorter wavelength is larger than that from the longer one because of ω^2-dependence

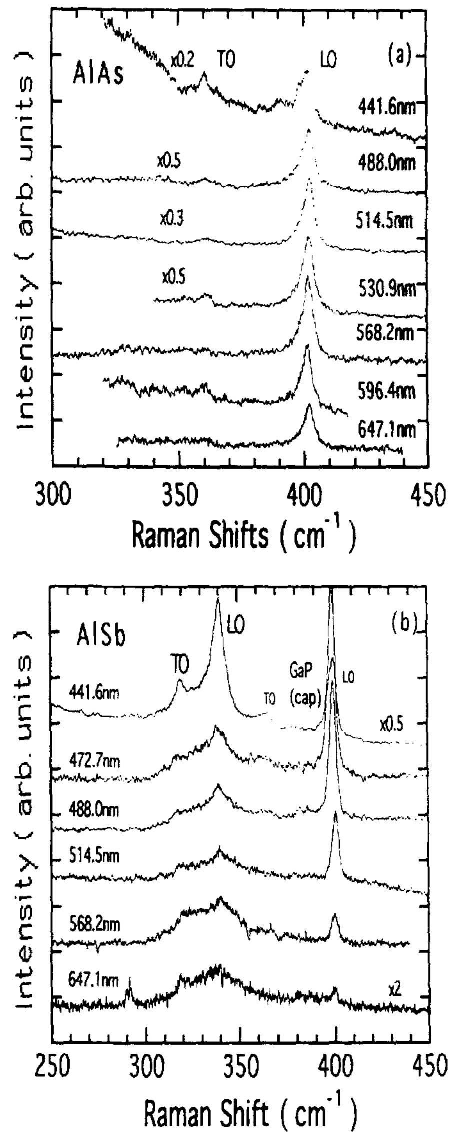

Fig. 3. Raman spectra for (a) AlAs ($x = 1$) and (b) AlSb ($x = 0$) measured by various wavelengths (647.1 to 441.6 nm) show obvious resonance scattering.

[17]. However, we notice that the Raman enhancements occur at 514.5 and 441.6 nm for AlAs and AlSb, respectively [see Figs 3(a) and 3(b)]. Such resonant scattering is often observed in *III–V* compound semiconductors. For analyzing the enhancement factor, we handled the actually absorbed power in the epilayer by eliminating the power absorption and reflection in the cap layer and interface. Additionally, the Raman intensity of a transparent BaF_2 crystal (T_{2g} mode at 240 cm^{-1}) is used for normalization. This simultaneously eliminates the ω^4-dependence and includes the combined spectral response of spectrometer and detector.

The relative Raman enhancements are then plotted in Fig. 4 vs incident photon energy. For the pure AlAs LO

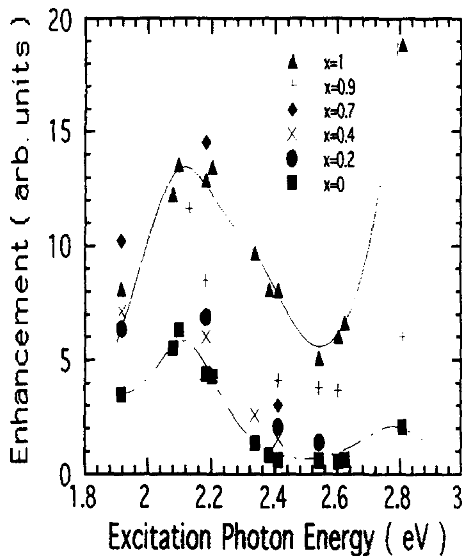

Fig. 4. The normalized enhancement of AlAsSb LO mode is shown vs excitation photon energy. Solid lines are calculated from equation (2) (see text).

mode (filled triangles), we see on the low energy side a clear enhancement peak at 2.15 eV that is a factor of 3 increment from 2.5 eV and a shoulder about 2.35 eV. The peak and shoulder photon energies can be ascribed to the indirect transitions of 2.15 and 2.35 eV from the Γ to X and L critical points, respectively. It excites the so-called outgoing resonance because the LO phonon energy is only 0.05 eV [18]. On the high energy side, as the excitation photon energy increases from 2.5 eV to 2.8 eV, the Raman enhancement sharply rises by 4 times. It is close to the direct E_0 transition at 3 eV, since we cannot obtain data beyond 2.8 eV with available laser source.

Similar enhancement is observed for the AlSb-LO mode (filled squares). There is a structure about 2.1 eV on the low energy side that shows more than a factor of 10 increment from 2.4 to 2.1 eV. This should correspond to the direct E_0 transition at 2.22 eV. Then a low-level region occurs between 2.4 and 2.6 eV, because of empty energy states from E_0 to E_1 (2.78 eV) gap at the Γ point. Here only the virtual transitions are involved in Raman scattering. On the high energy side, the enhancement increases gradually to 2.8 eV that is likely to be associated with the E_1 transition of AlSb.

The excitation profiles for AlAs and AlSb are indeed fitted well in Fig. 4 by the following formula that comprises the Lorentzian functions, [19]

$$\text{Enhancement}(E) \propto \sum_{j=0,1} \frac{A_j}{(E-E_j)^2 + \frac{\Gamma_j^2}{4}}. \quad (2)$$

Here j represents individual E_0 and E_1 transitions with respective amplitude A_j and width Γ_j. The best fitted widths range from 0.15 to 0.2 eV (see Fig. 4). For other $AlAs_xSb_{1-x}$ compositions, the resonance results appear to be large toward low photon energy of 2.1 eV as shown by the corresponding symbols, though the S/N ratios of these Raman data are poor. However, the enhancements should be related to the interband transitions in the vicinities of E_0 and E_1 critical points of $AlAs_xSb_{1-x}$, like the binary alloys.

In summary, we have used the Raman scattering to study the optic phonon properties of the ternary $AlAs_xSb_{1-x}$ compounds and observed the resonance effect in both TO and LO modes. The relative enhancements indicate that the E_0 and E_1 electronic transitions about 2.15 and 2.78 (or 3) eV are responsible for the resonant scattering. Our results also show one mode phonon behavior. Moreover, the spatial correlation mode can interpret the dependence of Raman shifts and widths on composition.

Acknowledgements—We are grateful for the supports from the National Science Council of R.O.C. under grant numbers NSC85-2112-M009-025 and 010.

REFERENCES

1. Williams, C.K., Glisson, T.H., Hauser, J.R. and Littlejohn, M.A., *J. Electron. Mater.*, **7,** 1978, 639.
2. Zinger, G.M., Ipatova, I.P. and Ryskin, A.I., *Sov. Phys. Semicond.*, **18,** 1984, 13.
3. Kurtz, S.R., Biefeld, R.M., Dawson, L.R., Baucom, K.C. and Howard, A.J., *Appl. Phys. Lett.*, **63,** 1994, 812.
4. Inata, T., Muto, S., Nakata, Y. and Fujii, T., *Jpn. J. Appl. Phys.*, **29,** 1990, 11382.
5. Chen, W.K. and Ou, J., *Jpn. J. Appl. Phys.*, **34,** 1995, L1581.
6. Biefeld, B.M., Allerman, A.A. and Pelczynski, M.W., *Appl. Phys. Lett.*, **68,** 1996, 932.
7. Sela, I., Bolognesi, C.R. and Kroemer, H., *Phys. Rev.*, **B46,** 1992, 16142.
8. Cherng, Y.T., Ma, K.Y. and Stringfellow, G.B., *Appl. Phys. Lett.*, **53,** 1988, 886.
9. Lucovsky, G., Cheng, K.Y. and Pearson, G.L., *Phys. Rev.*, **B12,** 1975, 4135.
10. Jou, M.J., Cherng, Y.T. and Stringfellow, G.B., *J. Appl. Phys.*, **64,** 1988, 1472.
11. Tiong, K.K., Amirtharaj, P.M., Pollak, F.H. and Aspnes, D.E., *Appl. Phys. Lett.*, **44,** 1983, 122.
12. Werninghaus, T., Hahn, J., Richter, F. and Zahn, D.R.T., *Appl. Phys. Lett.*, **70,** 1997, 958.
13. Chen, W.K., Ou, J. and Hsu, C.H., *Jpn. J. Appl. Phys.*, **35,** 1996, L1234.
14. Raptis, Y.S., Anastassakis, E. and Kanellis, G., *Phys. Rev.*, **B46,** 1992, 15801.
15. Saint-Cricq, N., Carles, R., Renucci, J.B., Zwick, A. and Renucci, M.A., *Solid State Commun.*, **39,** 1981, 1137.

16. Chang, I.F. and Mitra, S.S., *Advance in Physics*, **20,** 1971, 359.
17. Scott, J.F., Damen, T.C., Leite, R.C.C. and Silfvast, W.T., *Solid State Commun.*, **7,** 1969, 953.
18. Delaney, M.E., McGlinn, T.C., Klein, M.V. and Morkoc, H., *Phys. Rev.*, **B44,** 1991, 8605.
19. Bedel, E., Carles, E., Zwick, A., Renucci, J.B. and Renucci, M.A., *Phys. Rev.*, **B30,** 1984, 5923.